Coherent Forward Scattering Peak Induced by Anderson Localization

T. Karpiuk,[1,2] N. Cherroret,[3,4] K. L. Lee,[1] B. Grémaud,[1,4,5] C. A. Müller,[1] and C. Miniatura[1,5,6]

[1]*Centre for Quantum Technologies, National University of Singapore, 3 Science Drive 2, Singapore 117543, Singapore*
[2]*Wydział Fizyki, Uniwersytet w Białymstoku, ul. Lipowa 41, 15-424 Białystok, Poland*
[3]*Physikalisches Institut, Albert-Ludwigs-Universität Freiburg, Hermann-Herder-Str. 3, D-79104 Freiburg, Germany*
[4]*Laboratoire Kastler Brossel, Ecole Normale Supérieure, CNRS, UPMC; 4 Place Jussieu, 75005 Paris, France*
[5]*Department of Physics, National University of Singapore, 2 Science Drive 3, Singapore 117542, Singapore*
[6]*Institut Non Linéaire de Nice, UMR 7335, UNS, CNRS; 1361 route des Lucioles, 06560 Valbonne, France*

(Received 19 June 2012; published 7 November 2012)

Numerical simulations show that, at the onset of Anderson localization, the momentum distribution of a coherent wave packet launched inside a random potential exhibits, in the forward direction, a novel interference peak that complements the coherent backscattering peak. An explanation of this phenomenon in terms of maximally crossed diagrams predicts that the signal emerges around the localization time and grows on the scale of the Heisenberg time associated with the localization volume. Together, coherent back and forward scattering provide evidence for the occurrence of Anderson localization.

DOI: 10.1103/PhysRevLett.109.190601 PACS numbers: 05.60.Gg, 03.75.−b, 42.25.Dd, 72.15.Rn

Interference phenomena surviving statistical averages in spatially random media are of primary importance in order to understand the transport properties of bulk matter. Already in weakly disordered media, spectacular deviations from the conventional Boltzmann picture of transport have been discovered and studied. Important examples include weak localization and universal conductance fluctuations in mesoscopic electronic systems, or coherent backscattering (CBS) and intensity correlations in speckle patterns in the context of wave transport in disordered media [1]. In strongly scattering systems, transport can even be completely suppressed, due to Anderson localization (AL) [2,3]. For several years now, this phase-coherent inhibition of transport by disorder has been under active scrutiny in widely different systems using light [4], ultrasound [5], microwaves [6], and more recently ultracold atoms [7–12]. The observation of AL, however, remains a subtle issue, which requires accurate experiments, with a rather demanding control over absorption and decoherence.

In order to closely monitor the localization dynamics, we have recently proposed to study the momentum distribution of a coherent wave packet launched with finite velocity inside a random potential [13]. Phase-coherent multiple scattering is then clearly evidenced by the CBS peak, originating from the constructive interference of counterpropagating scattering amplitudes [14,15]. At the onset of AL, the amplitudes cease to propagate, so that the CBS peak should become stationary, an effect that we suggested to use as an indicator for AL [13]. The issue proves in fact much richer. In this Letter, we report numerical evidence that AL indeed leads to a stationary CBS signal, but also triggers the appearance of a novel, coherent forward scattering (CFS) peak in the opposite, *forward* direction. As a net effect, the momentum distribution shows a remarkable twin-peak structure (see Fig. 1).

We propose a theoretical explanation of CFS via a combination of the maximally crossed diagrams responsible for CBS. This theory implies that the CFS peak, while almost indiscernible for weak disorder in the diffusive regime, starts to rise around the localization time $\tau_{\rm loc} = \xi^2/D$ (ξ is the localization length and D the diffusion constant

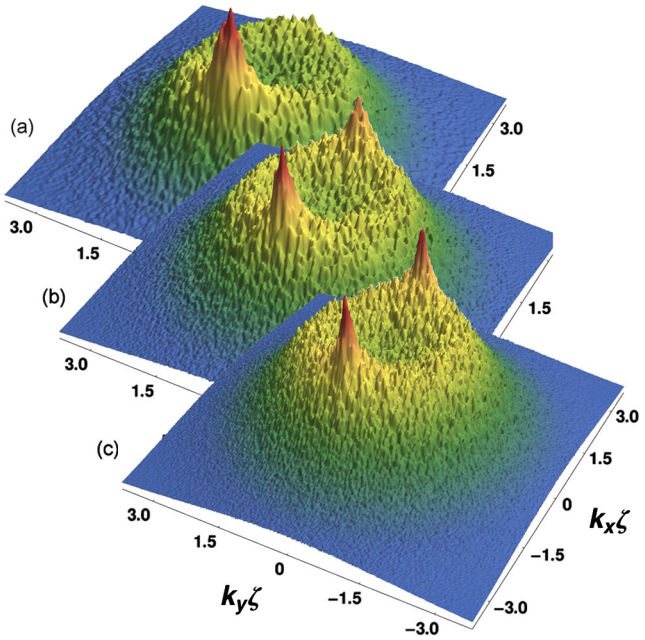

FIG. 1 (color online). Ensemble-averaged momentum distribution $\bar{n}(k_x, k_y, t)$ of a simulated matter wave launched with initial momentum $\boldsymbol{k}_0 = (1.5/\zeta, 0)$ inside a 2D random potential with correlation length ζ. The time unit is $\tau_\zeta = m\zeta^2/\hbar$. (a) $t = 10\tau_\zeta$: multiple scattering generates a coherent backscattering (CBS) peak at $-\boldsymbol{k}_0$. (b) $t = 90\tau_\zeta$: a coherent forward scattering (CFS) peak has emerged at $+\boldsymbol{k}_0$. (c) $t = 950\tau_\zeta$: the CBS and CFS twin peaks in the Anderson localization regime.

determined from the initially measured transport mean free path and time). Furthermore, we find that the CFS contrast grows on the scale of the Heisenberg time $\tau_H = h\nu\xi^d$ associated with the localization volume, where h is Planck's constant and ν the average density of states per unit volume. The CBS and CFS twin peaks are thus a clear signal for the occurrence of AL, and studying their dependence on system parameters and external fields promises further insights into wave dynamics in strongly disordered materials.

We consider, then, a quasimonochromatic wave packet that is prepared at time $t = 0$ with mean wave vector $\boldsymbol{k}_0$ and small spread $\Delta k \ll |\boldsymbol{k}_0|$ inside bulk disorder. In current cold-atom experiments [16,17], such a wave packet is produced with ultracold atoms released from a trap inside an optical speckle field [18]. The atoms can be suspended against gravity by a magnetic field gradient, and accelerated to the desired $\boldsymbol{k}_0$ by a suitable magnetic kick. After some time of evolution t inside the disorder, all fields are switched off, and the resulting momentum distribution $n(\boldsymbol{k}, t)$ is accessed by time-of-flight imaging.

We first study the matter wave dynamics by numerically solving the Schrödinger equation with Hamiltonian $H = \boldsymbol{p}^2/(2m) + V(\boldsymbol{r})$ in two dimensions (2D). Without loss of generality, $\overline{V(\boldsymbol{r})} = 0$, where the overbar denotes the ensemble average over disorder realizations. The pair correlation function $\overline{V(\boldsymbol{r})V(0)} = V^2 C(\boldsymbol{r}/\zeta)$ defines the potential strength via the variance V^2. It also specifies the spatial correlation length ζ, which defines a time scale $\tau_\zeta = m\zeta^2/\hbar$ and energy scale $E_\zeta = \hbar^2/(m\zeta^2)$ [19]. Figure 1 shows the momentum distribution at three different times, for a rather strong potential $V = 5E_\zeta$, averaged over 960 realizations of the speckle potential. The initial conditions are $\boldsymbol{k}_0 = (1.5/\zeta, 0)$ and $\Delta k = \sqrt{2}k_0/60 \approx 0.0236k_0$. At short times, in the diffusive regime [Fig. 1(a) for $t = 10\tau_\zeta$], the CBS peak at $-\boldsymbol{k}_0$ is the only distinctive feature. At longer times [Fig. 1(b) for $t = 90\tau_\zeta$], a CFS signal has risen at $+\boldsymbol{k}_0$. The CBS and CFS peaks then evolve toward a profile that remains stationary on the longest times accessible numerically [Fig. 1(c) for $t = 950\tau_\zeta$]. The peak contrasts, defined as height over background, are shown in Fig. 2 as a function of time. The rise of the CFS signal goes along with a reduction of the CBS contrast. In the long run, both contrasts converge to the same value. Similarly, the widths become comparable, and at the end of the time evolution covered here, the coherent signals appear as twin peaks. This progressive symmetrization of the momentum distribution is consistent with the expectation that it should become invariant under $\boldsymbol{k} \mapsto -\boldsymbol{k}$ at very long times because of time-reversal symmetry [20].

The remarkable symmetry between the two peaks suggests that CFS has the same physical origin as CBS, namely the interference of amplitudes counterpropagating along the same scattering path [21]. This interference contribution is a soft mode of central importance, known

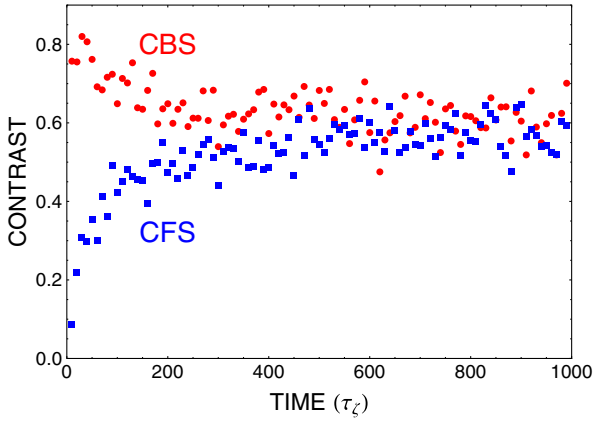

FIG. 2 (color online). Contrast of CBS (red circles) and CFS peak (blue squares) as a function of time, as obtained by fitting the data of Fig. 1 with the theoretical shapes, Eqs. (2) and (4), and a running average over a time window of $10\tau_\zeta$.

as the cooperon in mesoscopic systems [1]. Figure 3(a) represents the real-space trajectories associated with CBS. As shown in Fig. 3(b), a CFS signal can appear by concatenating two CBS processes, flipping twice the initial momentum and leading to an enhancement around $+\boldsymbol{k}_0$. Higher-order CFS (CBS) contributions can arise from chaining an even (odd) number of maximally crossed diagrams. The remaining question then is to understand why the CFS signal, while small in the diffusive regime, is boosted in the Anderson localization regime.

The quantitative analysis is simplified by assuming a very narrow initial momentum distribution $n(\boldsymbol{k}, t = 0) = (2\pi)^d \delta(\boldsymbol{k} - \boldsymbol{k}_0)$ (see below for the impact of a finite momentum spread $\Delta k > 0$). The ensemble-averaged momentum distribution at a later time t,

$$\bar{n}(\boldsymbol{k}, t) = \int \frac{dE}{2\pi} \int \frac{d\omega}{2\pi} e^{-i\omega t} \Phi_{\boldsymbol{k}\boldsymbol{k}_0 E}(\omega), \qquad (1)$$

is determined by the kernel $\Phi_{\boldsymbol{k}\boldsymbol{k}_0 E}$ of intensity propagation from initial momentum $\boldsymbol{k}_0$ to final momentum $\boldsymbol{k}$ via energy E. This kernel admits a well-known perturbation expansion in the weak-disorder regime [1]. The isotropic diffusive background is described by the series of ladder diagrams represented in Fig. 4(a), which results in a maximum

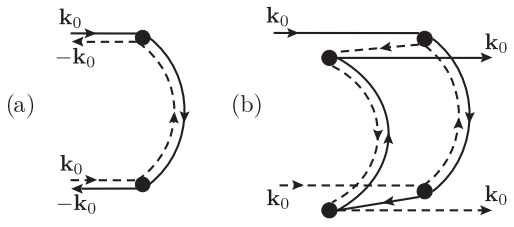

FIG. 3. Constructive interference of amplitudes along maximally crossed trajectories, leading to peaks at (a) $-\boldsymbol{k}_0$ for CBS and (b) $+\boldsymbol{k}_0$ for CFS, respectively.

background value of $\tau_s/(\hbar\pi\nu) \equiv n_{\mathrm{L}}$, where τ_s is the elastic scattering time [13].

The CBS contribution on top of the background is generated by the series of maximally crossed diagrams of Fig. 3(a). Its central ingredient is the diffusive cooperon $P_E(\omega, \boldsymbol{q}) = [-i\omega + D(E, \omega)\boldsymbol{q}^2]^{-1}$ that peaks around $\boldsymbol{q} = \boldsymbol{k}_0 + \boldsymbol{k} = 0$. In the diffusive regime $t \ll \tau_{\mathrm{loc}}$, $D(E)$ is independent of ω. The resulting CBS signal then has a decreasing width $(2Dt)^{-1/2}$, because the interfering amplitudes originate from points whose distance grows diffusively [13]. In the localization regime $t \gg \tau_{\mathrm{loc}}$, this diffusive expansion stops, and the diffusion constant obeys the scaling relation $D(E, \omega) \sim -i\omega\xi^2(E)$ [22]. Consequently, the CBS signal becomes a stationary Lorentzian

$$\bar{n}^{(\mathrm{C})}(\boldsymbol{k}) = \frac{n_{\mathrm{L}}}{1 + \xi^2(\boldsymbol{k} + \boldsymbol{k}_0)^2} + \bar{n}^{(1)}(k), \tag{2}$$

whose width is determined by the localization length $\xi(E_0)$, evaluated at the effective energy E_0 of the excitation with wave vector $\boldsymbol{k}_0$ inside the random medium. The second term in Eq. (2) is a negative background contribution that ensures particle-number conservation, $\int d\boldsymbol{k}\bar{n}^{(\mathrm{C})}(\boldsymbol{k}) = 0$. Technically, it is obtained by dressing the cooperon of Fig. 3(a) with additional impurity lines [1], commonly represented by the shaded 4-point Hikami box of Fig. 4(b) [23].

Let us now repeat this analysis for the CFS peak, which originates from the trajectories depicted in Fig. 3(b), involving the direct connection of two cooperons. Its contribution to the propagation kernel reads

$$\Phi^{(\mathrm{CC})}_{\boldsymbol{k}\boldsymbol{k}_0 E}(\omega) = \frac{A(\boldsymbol{k}, E)A(\boldsymbol{k}_0, E)}{(2\pi\nu)^2\tau_s}\int\frac{d\boldsymbol{q}}{(2\pi)^d}A(\boldsymbol{q}, E)P_E(\boldsymbol{q} + \boldsymbol{k}, \omega) \times P_E(\boldsymbol{q} + \boldsymbol{k}_0, \omega), \tag{3}$$

where $A(\boldsymbol{k}, E)$ is the spectral function [19] and d the spatial dimension. In the diffusive regime, a straightforward calculation shows that the CFS peak has a contrast in 2D of the order of $1/(k_0\ell)$, where ℓ denotes the transport mean free path. Thus, CFS is too weak to be visible in the weak-disorder regime $k_0\ell \gg 1$. In the localization regime, however, the scaling $D(\omega) \sim -i\omega\xi^2$ makes both cooperons singular and results in a signal that grows linearly in time:

$$\bar{n}^{(\mathrm{CC})}(\boldsymbol{k}, t) = 3n_{\mathrm{L}}\frac{t}{\tau_H}F_d(|\boldsymbol{k} - \boldsymbol{k}_0|\xi), \tag{4}$$

with $F_1(x) = 1/(4 + x^2)$, $F_2(x) = \mathrm{arcsinh}(x/2)/(\pi x\sqrt{4 + x^2})$, and $F_3(x) = \arctan(x/2)/(4\pi x)$. This CFS signal is indeed an interference peak centered at $+\boldsymbol{k}_0$ whose width is again given by the localization length, and whose contrast is of the order of t/τ_H.

Just as the CBS signal, the CFS contribution should also conserve the particle number. This leads us to dress the double cooperon with the 6-point Hikami box shown in Fig. 4(c). This diagram also appears in second-order weak localization corrections to the electronic conductivity [23]. As a result of summing 16 different contributions, Eq. (4) is modified to:

$$\bar{n}^{(\mathrm{CC})}(\boldsymbol{k}, t) = n_{\mathrm{L}}\frac{t}{\tau_H}F_d(|\boldsymbol{k} - \boldsymbol{k}_0|\xi) + \bar{n}^{(2)}(k, t), \tag{5}$$

where $\bar{n}^{(2)}(k, t)$ is a small negative background contribution that guarantees particle-number conservation, $\int d\boldsymbol{k}n^{(\mathrm{CC})}(\boldsymbol{k}, t) = 0$. In principle, there could be other isotropic contributions with an order of magnitude comparable to the CFS signal, such as the one depicted in Fig. 4(d), a combination of ladder and crossed series. But this contribution is exactly zero after proper dressing by the Hikami box. Similarly, other possible terms of the same order of magnitude vanish. This clearly identifies the class of diagrams 4(c) as the one responsible for the CFS peak in the Anderson localization regime.

We briefly evaluate the effect of a finite source coherence: the convolution of the signal (5) by a source distribution with width $\Delta k > 0$ reduces the contrast by a term of order $(\Delta k\xi)^2$. From our numerics for $V = 5E_\zeta$, we estimate $\xi \sim 8\zeta$ from the width of the CBS peak, such that the reduction remains small, $(\Delta k\xi)^2 \approx 0.1$. Having a coherent enough source with $\Delta k\xi \ll 1$ is thus mandatory to observe the CFS peak. In the opposite case, the CBS peak will have already decayed by the time AL sets in, now without producing any remarkable signature on the isotropic background.

Equation (5) implies that from $t \sim \tau_{\mathrm{loc}}$ onwards, the CFS peak rises to a contrast of order unity on the Heisenberg time scale $\tau_H = h\nu\xi^d$ associated with the localization volume. Figure 5 shows the growth of CFS at early times obtained numerically for different values of V. Using the CFS onset as a measure for the localization time, we show in the inset of Fig. 5 τ_{loc} as a function of V. The observed decrease agrees with the expectation that the localization time is smaller for stronger disorder. For the present parameters, spectral broadening is very important (cf. the

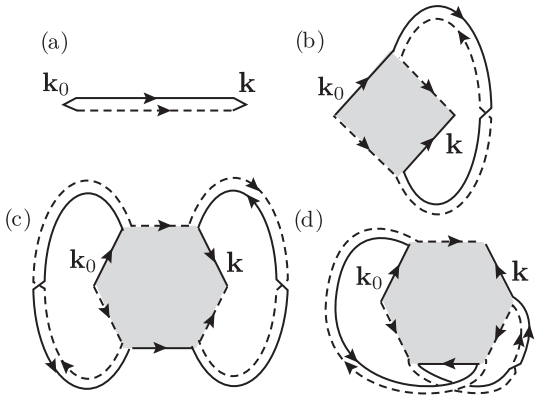

FIG. 4. Ladder (a) and maximally crossed (b) multiple scattering Feynman diagrams, giving rise to the diffusive background and the CBS signal, Eq. (2). Diagram (c) is responsible for the CFS peak, Eq. (5). Diagram (d) is exactly zero.

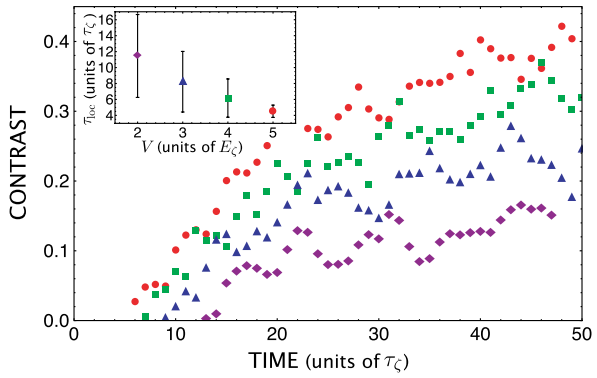

FIG. 5 (color online). Early-time CFS contrast for disorder strengths $V = 5E_\zeta$ (red circles), $V = 4E_\zeta$ (green squares), $V = 3E_\zeta$ (blue triangles), and $V = 2E_\zeta$ (purple diamonds). According to our theory, the CFS begins to rise when localization sets in. The inset shows $\tau_{\rm loc}$, estimated by the earliest CFS appearance, as a function of V.

broad background in Fig. 1). Consequently, the full signal is the sum of contributions from a rather wide range of energies, with lowest-energy components being localized first. A fully quantitative theory for the strong-disorder regime would require to know spectral densities, diffusion constants and localization lengths, which are not yet at hand for spatially correlated potentials.

Our numerics show that at long times $t > \tau_H$, the CBS and CFS contrasts saturate at a common value smaller than unity. This dynamics cannot be captured by our theoretical approach because it would require a summation of the full CBS and CFS series of repeated cooperons to all orders, including the dressing by higher-order Hikami boxes, which poses a formidable task. The failure of perturbative expansions beyond the Heisenberg time τ_H is anyhow well known, and one has to resort to other techniques like supersymmetry or random-matrix theory [24,25]. We expect, however, that the two salient features of our explanation, namely (i) the emergence of CFS around the localization time $\tau_{\rm loc}$ and (ii) a CBS and CFS dynamics on the Heisenberg time scale τ_H, remain valid. Indeed, a similar dynamics was predicted for the dynamical echo within weakly disordered quantum dots [26] and observed with ultrasound [27]. In our setup of bulk disorder, the confinement is due to AL, and the localization length stands for the effective system size. To our knowledge, it is an open question whether the CBS and CFS peaks can remain stationary or perhaps decay to a completely isotropic distribution on very long time scales associated with the glassy dynamics of the localization regime [28].

Future work should also address the impact of finite-size effects on the CFS signal. In many experiments, waves are sent through a scattering medium with open boundaries [4–6]. Especially for electromagnetic fields, quasi-plane-wave sources and detection of radiation patterns in the far field are readily available, enabling the clear observation of CBS in the reflected intensity [1]. We expect the CFS effect to be present as well in the transmitted intensity across a strongly localizing medium, but possibly difficult to observe because this requires good momentum resolution on the small transmitted signal.

In conclusion, we have discovered a coherent interference phenomenon that is induced by Anderson localization. It manifests itself as an interference peak with high visibility in the forward direction and is closely connected to the CBS peak. We have proposed a theoretical explanation by a combination of maximally crossed diagrams, and predicted CFS to occur in all dimensions $d = 1, 2, 3$. This effect provides an avenue for detailed investigations of AL in strongly random media, and should be in reach for current experiments with a good resolution in momentum space, such as cold atoms, excitons [29], polaritons [30], and photons [31].

We have benefitted from discussions with D. Delande and V. Savona, as well as with T. Bourdel and V. Josse and their colleagues. N. C. acknowledges financial support from the Alexander von Humboldt Foundation and hospitality by the Centre for Quantum Technologies (CQT), a Research Centre of Excellence funded by the Ministry of Education and the National Research Foundation of Singapore. Ch. M. and B. G. acknowledge funding from the CQT-CNRS LIA FSQL and from the France-Singapore Merlion program. Ch. M. is a Fellow of the Institute of Advanced Studies (NTU).

[1] E. Akkermans and G. Montambaux, *Mesoscopic Physics of Electrons and Photons* (Cambridge University Press, Cambridge, 2007).
[2] P. W. Anderson, Phys. Rev. **109**, 1492 (1958).
[3] *Mesoscopic Quantum Physics*, Proceedings of Les Houches Summer School, Session LXIV, edited by E. Akkermans, G. Montambaux, J. L. Pichard, and J. Zinn-Justin (Elsevier Science North Holland, Amsterdam, 1995).
[4] M. Störzer, P. Gross, C. M. Aegerter, and G. Maret, Phys. Rev. Lett. **96**, 063904 (2006).
[5] H. Hu, A. Strybulevych, J. H. Page, S. E. Skipetrov, and B. A. van Tiggelen, Nat. Phys. **4**, 945 (2008).
[6] A. A. Chabanov, M. Stoytchev, and A. Z. Genack, Nature (London) **404**, 850 (2000).
[7] L. Sanchez-Palencia and M. Lewenstein, Nat. Phys. **6**, 87 (2010); G. Modugno, Rep. Prog. Phys. **73**, 102 401 (2010).
[8] J. Chabé, G. Lemarié, B. Grémaud, D. Delande, P. Szriftgiser, and J.-C. Garreau, Phys. Rev. Lett. **101**, 255702 (2008); G. Lemarié, H. Lignier, D. Delande, P. Szriftgiser, and J.-C. Garreau, Phys. Rev. Lett. **105**, 090601 (2010).
[9] J. Billy, V. Josse, Z. Zuo, A. Bernard, B. Hambrecht, P. Lugan, D. Clément, L. Sanchez-Palencia, P. Bouyer, and A. Aspect, Nature (London) **453**, 891 (2008).

[10] G. Roati, C. D'Errico, L. Fallani, M. Fattori, C. Fort, M. Zaccanti, G. Modugno, M. Modugno, and M. Inguscio, Nature (London) **453**, 895 (2008).
[11] S. S. Kondov, W. R. McGehee, J. J. Zirbel, and B. DeMarco, Science **334**, 66 (2011).
[12] F. Jendrzejewski, A. Bernard, K. Müller, P. Cheinet, V. Josse, M. Piraud, L. Pezzé, L. Sanchez-Palencia, A. Aspect, and P. Bouyer, Nat. Phys. **8**, 398 (2012).
[13] N. Cherroret, T. Karpiuk, C. A. Müller, B. Grémaud, and C. Miniatura, Phys. Rev. A **85**, 011604(R) (2012).
[14] M. P. Van Albada and A. Lagendijk, Phys. Rev. Lett. **55**, 2692 (1985); P.-E. Wolf and G. Maret, *ibid.* **55**, 2696 (1985).
[15] G. Labeyrie, F. de Tomasi, J.-C. Bernard, C. A. Müller, C. Miniatura, and R. Kaiser, Phys. Rev. Lett. **83**, 5266 (1999).
[16] G. Labeyrie, T. Karpiuk, B. Grémaud, C. Miniatura, and D. Delande, arXiv:1206.0845.
[17] F. Jendrzejewski, K. Müller, J. Richard, A. Date, T. Plisson, P. Bouyer, A. Aspect, and V. Josse, Phys. Rev. Lett. (to be published).
[18] D. Clément, A. F. Varón, J. A. Retter, L. Sanchez-Palencia, A. Aspect, and P. Bouyer, New J. Phys. **8**, 165 (2006).
[19] R. C. Kuhn, C. Miniatura, D. Delande, O. Sigwarth, and C. A. Müller, Phys. Rev. Lett. **95**, 250403 (2005); R. C. Kuhn, O. Sigwarth, C. Miniatura, D. Delande, and C. A. Müller, New J. Phys. **9**, 161 (2007).
[20] R. Zimmermann, E. Runge, and V. Savona, in *Quantum Coherence, Correlation and Decoherence in Semiconductor Nanostructures*, edited by T. Takagahara (Elsevier Science, Oxford, 2003).
[21] A forward peak for point scatterers due to recurrent scattering in the weak-disorder regime has been predicted by B. van Tiggelen, A. Lagendijk, and A. Tip, J. Phys. Condens. Matter **2**, 7653 (1990). For the speckle potential considered here, recurrent scattering is absent. Moreover, we have checked that Gaussian disorder also produces CFS.
[22] D. Vollhardt and P. Wölfle, in *Electronic Phase Transitions*, edited by W. Hanke and Ya. V. Kopaev (North-Holland, Amsterdam, 1992), Chap. 1, p. 1.
[23] S. Hikami, Phys. Rev. B **24**, 2671 (1981).
[24] K. B. Efetov, *Supersymmetry in Disorder and Chaos* (Cambridge University Press, Cambridge, 1997).
[25] C. W. J. Beenakker, Rev. Mod. Phys. **69**, 731 (1997).
[26] V. N. Prigodin, B. L. Altshuler, K. B. Efetov, and S. Iida, Phys. Rev. Lett. **72**, 546 (1994).
[27] R. L. Weaver and O. I. Lobkis, Phys. Rev. Lett. **84**, 4942 (2000).
[28] A. D. Mirlin, Phys. Rep. **326**, 259 (2000).
[29] W. Langbein, E. Runge, V. Savona, and R. Zimmermann, Phys. Rev. Lett. **89**, 157401 (2002).
[30] A. Amo, J. Lefrère, S. Pigeon, C. Adrados, C. Ciuti, I. Carusotto, R. Houdré, E. Giacobino, and A. Bramati, Nat. Phys. **5**, 805 (2009).
[31] T. Schwartz, G. Bartal, S. Fishman, and M. Segev, Nature (London) **446**, 52 (2007).